

Superconductivity induced by the inter-valley Coulomb scattering in a few layers of graphene

Tommaso Cea

Department of Physical and Chemical Sciences, Università degli Studi dell'Aquila, I-67100 L'Aquila, Italy

We study the inter-valley scattering induced by the Coulomb repulsion as a purely electronic mechanism for the origin of superconductivity in few layers of graphene. The pairing is strongly favored by the presence of van Hove singularities (VHS's) in the density of states (DOS). We consider three different heterostructures: twisted bilayer graphene (TBG), rhombohedral trilayer graphene (RTG) and Bernal bilayer graphene (BBG). We obtain trends and estimates of the superconducting (SC) critical temperature in agreement with the experimental findings, which might identify the inter-valley Coulomb scattering as a universal pairing mechanism in few layers of graphene.

I. INTRODUCTION

The discovery of superconductivity in TBG[1–3] led the scientific community to a renewed interest in the study of the SC properties of graphene, that has been further motivated by the more recent observations of SC behavior in other heterostructures based on graphene: twisted trilayer graphene (TTG)[4], untwisted RTG[5] and BBG[6] in a perpendicular electric field. In all these systems the SC transition can be controlled by experimentally tunable parameters, like eg: the relative twist between the layers, the electronic density and the applied displacement field. Even though the critical temperatures, T_c , observed so far in these materials do not exceed the scale of a few Kelvin, the large ratios between T_c and the Fermi energy, up to $\sim 10\%$, suggests that a strong pairing interaction is at play. On the other hand, the complex phase diagrams reported in the literature clearly highlight the strongly correlated behavior. The recent observation of the Ref. [7], that the value of T_c in BBG can be increased by one order of magnitude by a substrate of WSe_2 , emphasizes the highly tunable nature of the pairing, paving the way towards engineering new techniques for controlling the magnitude of T_c . Furthermore, the violation of the Pauli's limit reported in the experiments [4–6] suggests that spin-triplet Cooper pairs are favored in these systems.

On the theoretical side, it is universally accepted that the band flattening and the vicinity of the VHS's to the Fermi level enhance the role of the electronic interactions in TBG, TTG, RTG and BBG, favoring the formation of symmetry broken phases (see eg the Refs. [8–13]). However, the debate on the mechanism at the origin of the superconductivity in these systems is still open. Many models have been studied so far, that either consider the superconductivity driven by purely electronic interactions[9, 12, 14–32] or by more conventional phononic mechanisms[33–43]. The combined effects of the screened Coulomb interaction, the electronic Umklapp processes and the electron-phonon coupling have been shown to favor the pairing in TBG[44–46] and in TTG[47]. Furthermore, the Refs. [48–52] explored other unconventional mechanisms, in which the pairing is mediated by soft electronic collective modes. Remarkably,

there is not yet a general agreement on whether the superconductivity observed in TBG and in TTG has the same origin as in the untwisted RTG and BBG.

In this article, we study the inter-valley scattering induced by the Coulomb interaction as a purely electronic mechanism for the origin of superconductivity in few layers of graphene. The resulting Cooper pairs are spin-triplets with the two electrons in opposite valleys, K, K' , featuring p - or f -wave symmetry. Because the large momentum transfer, $\Delta K \equiv K - K'$, involved in the process makes the interaction strength negligible, a high DOS is necessary to boost the pairing. This condition is often realized in few layers of graphene, where the electronic bands can be flattened by tuning a number of experimental parameters, thus giving rise to VHS's. At first approximation, we neglect the contribution of the intra-valley Coulomb repulsion, which is long-ranged, since it is drastically screened in the van Hove scenario. We show quantitatively that this assumption is fully justified in the SI[53]. Using effective continuum models with realistic parameters, we characterize the SC transition induced by the inter-valley Coulomb scattering in TBG, RTG and BBG, upon varying the relative twist between the layers and/or the electronic density and/or the displacement field. We obtain estimates and trends of T_c in good agreement with the experimental results, emphasizing the strong enhancement of T_c by the presence of VHS's. Remarkably, our calculations account for the different orders of magnitude of the critical temperatures observed in different materials. Considering also the experimental evidence of spin-triplet superconductivity in these systems, our study might identify the inter-valley Coulomb scattering as a universal driving mechanism for the superconductivity observed so far in few layers of graphene. We also identify a non-trivial structure of the SC order parameter (OP) in real space.

II. THE MODEL: EFFECTIVE ATTRACTION FROM THE INTER-VALLEY SCATTERING

Our theoretical description of the pairing interaction starts from considering the Coulomb repulsion between the p_z electrons within the minimal lattice model for a

multilayer of graphene:

$$\hat{H}_{int} = \frac{1}{2} \sum_{\mathbf{R}\mathbf{R}'} \sum_{ij\sigma\sigma'} c_{i\sigma}^\dagger(\mathbf{R}) c_{j\sigma'}^\dagger(\mathbf{R}') V_C^{ij}(\mathbf{R} - \mathbf{R}') c_{j\sigma'}(\mathbf{R}') c_{i\sigma}(\mathbf{R}), \quad (1)$$

where \mathbf{R} are the coordinates of the Bravais lattice, i, j are the labels of the sub-lattice/layer, $c_{i\sigma}(\mathbf{R})$ is the quantum operator for the annihilation of one electron with spin σ in the p_z orbital localized at the position $\mathbf{R} + \boldsymbol{\delta}_i$, $\boldsymbol{\delta}_i$ being the internal coordinate in the unit cell, and:

$$V_C^{ij}(\mathbf{R} - \mathbf{R}') = \frac{e^2}{4\pi\epsilon |\mathbf{R} - \mathbf{R}' + \boldsymbol{\delta}_i - \boldsymbol{\delta}_j|} \quad (2)$$

is the Coulomb potential, where e is the electron charge and ϵ is the dielectric constant of the environment, $\epsilon = \epsilon_0$

in the vacuum. Next, we consider the continuum limit of the lattice model, by expanding the operators c as:

$$c_{i\sigma}(\mathbf{R}) \equiv A_c^{1/2} \left[\psi_{i\sigma}^K(\mathbf{R}) e^{i\mathbf{K}\cdot\mathbf{R}} + \psi_{i\sigma}^{K'}(\mathbf{R}) e^{i\mathbf{K}'\cdot\mathbf{R}} \right], \quad (3)$$

where $A_c = \sqrt{3}a^2/2$ is the area of the unit cell of graphene, $a = 2.46\text{\AA}$ being the lattice constant, \mathbf{K}, \mathbf{K}' are the non equivalent corners of the BZ and $\psi_{i\sigma}^K(\mathbf{r}), \psi_{i\sigma}^{K'}(\mathbf{r})$ are fermionic operators, which vary smoothly with the continuum position, \mathbf{r} , and represent the valley projections of $c_{i\sigma}(\mathbf{R})$. Replacing the Eq. (3) into the Eq. (1), among all the terms one finds the following valley-exchange interaction:

$$\hat{H}_{exc} = A_c^2 \sum_{\mathbf{R}\mathbf{R}'} \sum_{ij\sigma\sigma'} \psi_{i\sigma}^{K,\dagger}(\mathbf{R}) \psi_{j\sigma'}^{K',\dagger}(\mathbf{R}') \psi_{j\sigma'}^K(\mathbf{R}') \psi_{i\sigma}^{K'}(\mathbf{R}) V_C^{ij}(\mathbf{R} - \mathbf{R}') e^{-i\Delta\mathbf{K}\cdot(\mathbf{R}-\mathbf{R}')}, \quad (4)$$

which describes the inter-valley scattering processes. As we show in detail in the supplementary information (SI)[53], the Eq. (4) can be safely approximated by the continuum Hamiltonian:

$$\hat{H}_{exc} \simeq -J \sum_{i\sigma\sigma'} \int d^2\mathbf{r} \psi_{i\sigma}^{K,\dagger}(\mathbf{r}) \psi_{i\sigma'}^{K',\dagger}(\mathbf{r}) \psi_{i\sigma}^{K'}(\mathbf{r}) \psi_{i\sigma'}^K(\mathbf{r}), \quad (5)$$

where: $J \equiv \frac{e^2}{2\epsilon|\Delta\mathbf{K}|}$ is the Fourier transform of the Coulomb potential in 2D, evaluated at $\Delta\mathbf{K}$. It's worth noting that the interaction described by the Eq. (5) is purely local, not only in the space coordinates, but also in the sub-lattice and layer indices. Because $J > 0$, \hat{H}_{exc} provides an effective attraction in the spin-triplet channel (see the SI[53]), favoring the Cooper pairing with electrons in opposite valleys. This kind of interaction belongs to the universality class identified by Crepel and Fu[54, 55], who have demonstrated the relevance of the valley-exchange interaction in inducing the pairing in narrow band systems. As we already mentioned, we stress that the spin triplet superconductivity is a general claim of the experimental works. On the other hand, the valley-exchange from the Coulomb interaction has been shown to favor spin-triplet superconductivity in various materials (see for example the Refs. [29, 56, 57]). The SC OP, $\Delta^i(\mathbf{r})$, is purely local and the value of T_c can be obtained within the BCS theory as the largest temperature for which it exists a nonzero solution of the linearized

gap equation:

$$\Delta^i(\mathbf{r}) = \frac{J}{\beta} \sum_j \int d\mathbf{r}' \sum_{l=-\infty}^{+\infty} \times \times \mathcal{G}_{ij}^K(\mathbf{r}, \mathbf{r}'; i\omega_l) \mathcal{G}_{ij}^{K'}(\mathbf{r}, \mathbf{r}'; -i\omega_l) \Delta^j(\mathbf{r}'), \quad (6)$$

where $\beta = (K_B T)^{-1}$ is the inverse of the temperature, $\omega_l = \pi(2l+1)/(\hbar\beta)$ are fermionic Matsubara frequencies and $\mathcal{G}^{K,K'}$ are the Green's function for the K, K' valleys, respectively, computed in the normal phase. The Eq. (6) is written in real space in order to be as general as possible, holding also for non-translationally invariant systems, as is the case of the TBG that we will consider below.

It's worth noting that: i) J is generally small. For example, if we consider $\epsilon/\epsilon_0 = 4$, which mimics the screening by a substrate of hBN, then $J \simeq 13.25\text{eV}\text{\AA}^2$, consistent with the estimates of the Hubbard interaction strength in graphene[58–62]. Such a small value requires a large DOS at the Fermi energy, N_F , for making the dimensionless SC coupling, $\lambda = N_F J$, sizeable. While the DOS is suppressed in the monolayer graphene close to charge neutrality, multilayer stacks of graphene offer a way to increase the value of N_F , and hence to strengthen λ , upon tuning a number of experimental parameters, like eg the relative twist between the layers, the electronic density, the displacement field etc.; ii) we are not considering the effects of the intra-valley scattering induced by

the Coulomb interaction at small momenta, which are repulsive. In a van Hove scenario, these terms are suppressed by the strong internal screening. As we show in the SI[53] for the case of the RTG, the strength of the screened intra-valley Coulomb repulsion is orders of magnitude smaller than J , which fully justifies its omission; iii) we are not considering the internal screening of J , which is supposed to be negligible as it is induced by the particle-hole excitations with the particle and the hole in opposite valleys. These kind of processes are indeed suppressed despite of a large DOS. This assumption is justified quantitatively in the SI[53], where we show that the screening essentially does not affect the value of J as compared to its bare value.

III. RESULTS

The case of the TBG. A relative small twist, θ , between the two layers of a bilayer graphene generates a moiré superlattice with periodicity: $L_m \simeq a/\theta$, much larger than the lattice constant of the monolayer graphene. The inter-layer hopping varies smoothly at the scale of the moiré, breaking the translational invariance within each moiré unit cell and strongly hybridizing the p_z orbitals of the constitutive graphene sheets. The superconductivity has been observed at the "magic" angle, $\theta = 1.05^\circ$ [1–3], where the free electron spectrum features two weakly dispersing narrow bands at the charge neutrality point (CNP), generating strong VHS's in the DOS[63, 64].

Using the continuum model of the TBG[63–66], we solve the linearized gap equation (6) as detailed in the SI[53]. The Fig. 1 shows T_c as a function of the filling per moiré unit cell, ν , obtained for three values of the twist angle, as coded in the caption, and for $\epsilon/\epsilon_0 = 4$. We find values of T_c of the order of 1K, in good agreement with the experimental findings. T_c is the largest for $\theta = 1.05^\circ$, where the bandwidth at the CNP is minimum. The band structure and the DOS corresponding to the two central bands of the TBG at $\theta = 1.05^\circ$ are shown in the Fig. 2 for: $\nu = -1, 0, 1$. The continuous and the dashed lines refer to the K and K' valleys, respectively, while the horizontal lines identify the Fermi energies. Note that the reshaping of the bands with the filling is induced by the Hartree corrections[8, 10]. Comparing the Figs. 1 and 2 makes it clear that the value of T_c increases with N_F , which explains why we obtain the largest T_c at $\nu = 0$, where the bandwidth is minimum. It's worth noting that the TBG is actually a flavor polarized insulator at $\nu = 0$. As we are not considering flavor polarized phases, the superconductivity that we obtain at $\nu = 0$ is not realistic. Nonetheless, it serves as an example to grab the relevance of the VHS's in inducing the pairing. As we show in the SI[53], the order of magnitude of T_c and its ν -dependence do not change for realistic values of the external screening: $\epsilon/\epsilon_0 \sim 4 - 6$.

The OP, $\Delta^i(\mathbf{r})$, that we obtain as solution of the Eq.

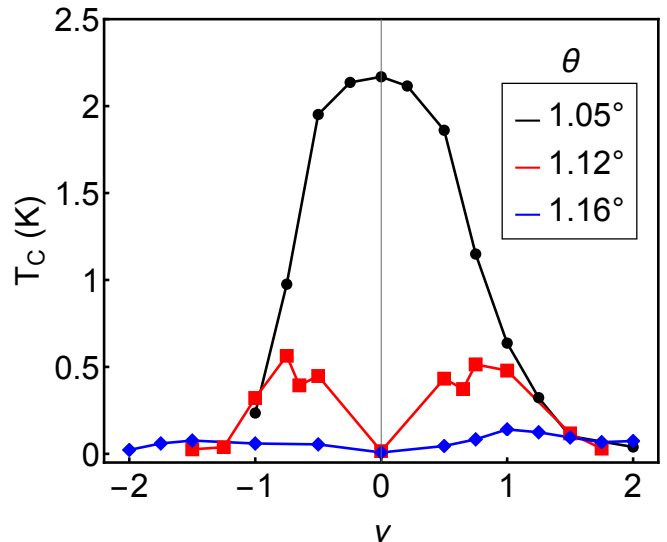


Figure 1. T_c as a function of the filling, obtained for: $\epsilon/\epsilon_0 = 4$ and $\theta = 1.05^\circ, 1.12^\circ, 1.16^\circ$.

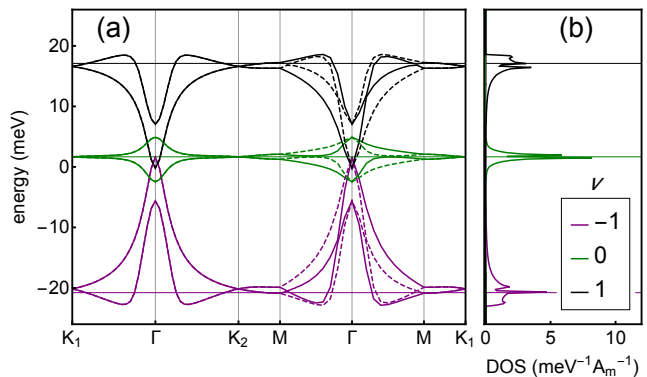


Figure 2. Band structure (a) and DOS (b) corresponding to the two central bands of the TBG, obtained for: $\theta = 1.05^\circ$ and $\nu = -1, 0, 1$. The continuous and the dashed lines refer to the K and K' valleys, respectively, while the horizontal lines identify the Fermi energies. The DOS is expressed in units of $\text{meV}^{-1}A_m^{-1}$, where $A_m = \sqrt{3}L_m^2/2$ is the area of the moiré unit cell.

(6) at $T = T_c$, is almost uniform in the sub-lattices and layers, has a constant phase and varies in the moiré unit cell, reaching its maxima in the regions with local AA stacking. Maps of $\Delta^i(\mathbf{r})$ are shown in the SI[53].

The case of the RTG and BBG. Both RTG and BBG become superconductors at very low electronic densities: $n_e \sim 10^{12}\text{cm}^{-2}$, when an electric field is applied perpendicular to the graphene's flakes[5, 6]. The experimental T_c 's are $\sim 10^{-1}\text{K}$ for the RTG and $\sim 10^{-2}\text{K}$ for the BBG. From the electronic point of view, a perpendicular electric field breaks the inversion symmetry and gaps out the Dirac points in both RTG and BBG. The nearly flat dispersion close to the gap's edge gives rise to a pronounced VHS. For values of n_e close to those

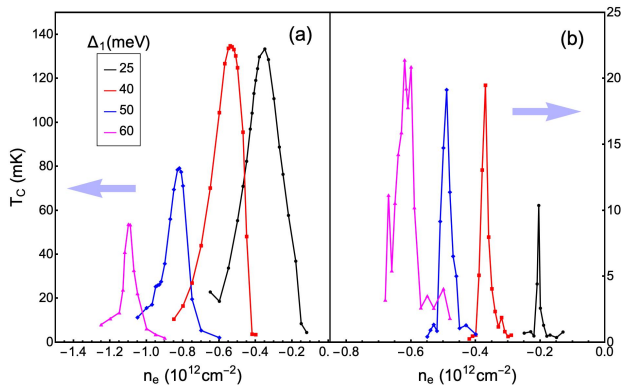


Figure 3. T_c of the hole-doped RTG (a) and BBG (b) as a function of n_e , obtained for: $\epsilon/\epsilon_0 = 4$ and Δ_1 as coded in the inset panel.

at which the superconductivity has been reported, the Fermi level lies near the VHS.

We study the low energy continuum model of the RTG and BBG, with the hopping amplitudes given by the Refs. [28, 67, 68], and an inter-layer bias, Δ_1 , describing the perpendicular electric field (see the SI[53]). We extract T_c by using the linearized gap equation (6) in the translationally invariant case, as detailed in the SI[53]. The Fig. 3 shows the values of T_c as a function of n_e in the hole-doped RTG (a) and BBG (b), obtained for: $\epsilon/\epsilon_0 = 4$ and realistic values of Δ_1 , as coded in the inset panel. We obtain critical temperatures up to $\sim 130 - 140$ mK for the RTG, and up to ~ 20 mK for the BBG, approximately one order of magnitude smaller than in RTG. The peak's intensity and position depend on Δ_1 . These estimates of T_c are in excellent agreement with the two experiments [5, 6]. The Ref. [5] identifies two distinct SC phases of the RTG, named SC1 and SC2. While the former does respect the Pauli's limit, the latter does not, implying that the pairing is spin-unpolarized in SC1 and spin-polarized in SC2. The superconductivity observed in the BBG in the Ref. [6] is always accompanied by the violation of the Pauli's limit, suggesting that the SC1 phase is absent in the BBG. It's worth noting that the spin-triplet pairing that we are considering is compatible with both spin-unpolarized and spin-polarized Cooper pairs, and consequently it does not exclude a priori either the SC1 or the SC2 regime. However, comparing the values of T_c in the Fig. 3(a) with the experimental temperatures reported in the Ref. [5], it seems that our calculations are missing the SC2 phase of the RTG. Remarkably, our results reproduce quite well both the range of n_e in which the superconductivity has been reported and the narrowness of the SC domain. The Fig. 4 shows the band structure (a) and DOS (b) of the RTG close to the CNP, obtained for the values of Δ_1 considered in the Fig. 3 and color coded as there. The bands flatten close to the gap edge,

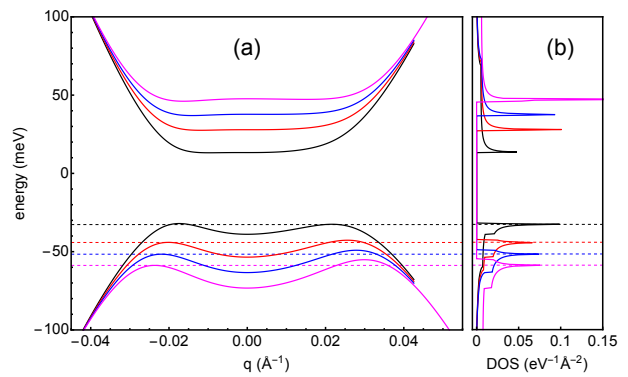


Figure 4. Band structure (a) and DOS (b) of the RTG close to the CNP, obtained for: $\Delta_1 = 25, 40, 50, 60$ meV, and color coded as in the Fig. 3. Here $q = 0$ at the K point. The horizontal dashed lines indicate the Fermi levels corresponding to the densities that maximize T_c in the Fig. 3.

giving rise to the VHS's in the DOS, whose position and intensity can be tuned by Δ_1 . The horizontal dashed lines indicate the Fermi levels corresponding to the densities that maximize T_c in the Fig. 3, emphasizing that the superconductivity is strongly favored when the Fermi level matches the VHS. The spectral feature of the BBG in the presence of a perpendicular electric field is qualitatively very similar to that of the RTG. The narrowness of the SC domain can be explained by considering that the bands of the RTG and BBG remain rigid upon tuning n_e , that only moves the Fermi level. Thus, there is only a small range of values of n_e for which the Fermi level lies near the VHS. This is in stark contrast to the case of the TBG, where the shape of the bands changes with the filling in order to pin the VHS to the Fermi level[8, 10], then allowing for wide SC domains.

Finally, we find that the SC OP is fully localized in the layer and sub-lattice in which the electric field confines the low energy electrons, as shown in the Ref. [69].

IV. CONCLUSIONS

Our work represents one step further in the study of the origin of the superconductivity recently observed in few layers of graphene, that can be explained by a universal purely electronic mechanism, in which the valley-exchange induced by the Coulomb repulsion serves as the pairing glue in the valley-singlet/spin-triplet Cooper channel. The pairing is then favored by the proximity of the Fermi level to the VHS's, that can be achieved in these materials by tuning a set of experimental parameters. Exploiting low energy continuum models, we provide a general method for computing the SC critical temperature as well as the symmetry of the OP, and we test it in three representative systems: TBG, RTG and BBG, obtaining an excellent agreement with the experimental findings. Beyond the case of the graphene-

based heterostructures, our analysis might be generalized to study the pairing in the wider class of materials displaying valley degrees of freedom and VHS's, as is the case of the recently discovered superconductors on Silicene surface[70–72].

V. ACKNOWLEDGEMENTS

We thank Francisco Guinea and Nicolás Defenu for useful discussions. We acknowledge fundings from the European Commission, under the Graphene Flagship, Core 3, grant number 881603.

-
- [1] Y. Cao, V. Fatemi, S. Fang, K. Watanabe, T. Taniguchi, E. Kaxiras, and P. Jarillo-Herrero, Unconventional superconductivity in magic-angle graphene superlattices, *Nature* **556**, 43 (2018).
- [2] X. Lu, P. Stepanov, W. Yang, M. Xie, M. A. Aamir, I. Das, C. Urgell, K. Watanabe, T. Taniguchi, G. Zhang, A. Bachtold, A. H. MacDonald, and D. K. Efetov, Superconductors, orbital magnets and correlated states in magic-angle bilayer graphene, *Nature* **574**, 653 (2019).
- [3] M. Yankowitz, S. Chen, H. Polshyn, Y. Zhang, K. Watanabe, T. Taniguchi, D. Graf, A. F. Young, and C. R. Dean, Tuning superconductivity in twisted bilayer graphene, *Science* **363**, 1059 (2019), <https://science.sciencemag.org/content/363/6431/1059.full.pdf>.
- [4] J. M. Park, Y. Cao, K. Watanabe, T. Taniguchi, and P. Jarillo-Herrero, Tunable strongly coupled superconductivity in magic-angle twisted trilayer graphene, *Nature* **590**, 249 (2021).
- [5] H. Zhou, T. Xie, T. Taniguchi, K. Watanabe, and A. F. Young, Superconductivity in rhombohedral trilayer graphene, *Nature* **598**, 434 (2021).
- [6] H. Zhou, L. Holleis, Y. Saito, L. Cohen, W. Huynh, C. L. Patterson, F. Yang, T. Taniguchi, K. Watanabe, and A. F. Young, Isospin magnetism and spin-polarized superconductivity in bernal bilayer graphene, *Science* **375**, 774 (2022), <https://www.science.org/doi/pdf/10.1126/science.abm8386>.
- [7] Y. Zhang, R. Polski, A. Thomson, É. Lantagne-Hurtubise, C. Lewandowski, H. Zhou, K. Watanabe, T. Taniguchi, J. Alicea, and S. Nadj-Perge, Spin-Orbit Enhanced Superconductivity in Bernal Bilayer Graphene, arXiv e-prints , arXiv:2205.05087 (2022), [arXiv:2205.05087 \[cond-mat.supr-con\]](https://arxiv.org/abs/2205.05087).
- [8] F. Guinea and N. R. Walet, Electrostatic effects, band distortions, and superconductivity in twisted graphene bilayers, *Proceedings of the National Academy of Sciences* **115**, 13174 (2018), <https://www.pnas.org/doi/pdf/10.1073/pnas.1810947115>.
- [9] Y. Sherkunov and J. J. Betouras, Electronic phases in twisted bilayer graphene at magic angles as a result of van hove singularities and interactions, *Phys. Rev. B* **98**, 205151 (2018).
- [10] T. Cea, N. R. Walet, and F. Guinea, Electronic band structure and pinning of fermi energy to van hove singularities in twisted bilayer graphene: A self-consistent approach, *Phys. Rev. B* **100**, 205113 (2019).
- [11] T. Cea and F. Guinea, Band structure and insulating states driven by coulomb interaction in twisted bilayer graphene, *Phys. Rev. B* **102**, 045107 (2020).
- [12] Y.-P. Lin and R. M. Nandkishore, Parquet renormalization group analysis of weak-coupling instabilities with multiple high-order van hove points inside the brillouin zone, *Phys. Rev. B* **102**, 245122 (2020).
- [13] D. V. Chichinadze, L. Classen, Y. Wang, and A. V. Chubukov, Cascade of transitions in twisted bilayer graphene – the Van Hove scenario, arXiv e-prints , arXiv:2206.10539 (2022), [arXiv:2206.10539 \[cond-mat.mes-hall\]](https://arxiv.org/abs/2206.10539).
- [14] H. Isobe, N. F. Q. Yuan, and L. Fu, Unconventional superconductivity and density waves in twisted bilayer graphene, *Phys. Rev. X* **8**, 041041 (2018).
- [15] C.-C. Liu, L.-D. Zhang, W.-Q. Chen, and F. Yang, Chiral spin density wave and $d + id$ superconductivity in the magic-angle-twisted bilayer graphene, *Phys. Rev. Lett.* **121**, 217001 (2018).
- [16] J. González and T. Stauber, Kohn-luttinger superconductivity in twisted bilayer graphene, *Phys. Rev. Lett.* **122**, 026801 (2019).
- [17] Y.-Z. You and A. Vishwanath, Superconductivity from valley fluctuations and approximate so(4) symmetry in a weak coupling theory of twisted bilayer graphene, *npj Quantum Materials* **4**, 16 (2019).
- [18] B. Roy and V. Juričić, Unconventional superconductivity in nearly flat bands in twisted bilayer graphene, *Phys. Rev. B* **99**, 121407 (2019).
- [19] G. Sharma, M. Trushin, O. P. Sushkov, G. Vignale, and S. Adam, Superconductivity from collective excitations in magic-angle twisted bilayer graphene, *Phys. Rev. Research* **2**, 022040 (2020).
- [20] D. V. Chichinadze, L. Classen, and A. V. Chubukov, Nematic superconductivity in twisted bilayer graphene, *Phys. Rev. B* **101**, 224513 (2020).
- [21] W. Qin, B. Zou, and A. H. MacDonald, Critical magnetic fields and electron-pairing in magic-angle twisted bilayer graphene, arXiv e-prints , arXiv:2102.10504 (2021), [arXiv:2102.10504 \[cond-mat.supr-con\]](https://arxiv.org/abs/2102.10504).
- [22] Z. Dong and L. Levitov, Activating superconductivity in a repulsive system by high-energy degrees of freedom, arXiv e-prints , arXiv:2103.08767 (2021), [arXiv:2103.08767 \[cond-mat.supr-con\]](https://arxiv.org/abs/2103.08767).
- [23] A. Ghazaryan, T. Holder, M. Serbyn, and E. Berg, Unconventional superconductivity in systems with annular fermi surfaces: Application to rhombohedral trilayer graphene, *Phys. Rev. Lett.* **127**, 247001 (2021).
- [24] H. Dai, J. Hou, X. Zhang, Y. Liang, and T. Ma, Mott insulating state and $d + id$ superconductivity in an abc graphene trilayer, *Phys. Rev. B* **104**, 035104 (2021).
- [25] J. Gonzalez and T. Stauber, Ising superconductivity induced from valley symmetry breaking in twisted trilayer graphene, arXiv e-prints , arXiv:2110.11294 (2021), [arXiv:2110.11294 \[cond-mat.supr-con\]](https://arxiv.org/abs/2110.11294).
- [26] A. Fischer, Z. A. H. Goodwin, A. A. Mostofi, J. Lischner, D. M. Kennes, and L. Klebl, Unconventional superconductivity in magic-angle twisted trilayer graphene, *npj Quantum Materials* **7**, 5 (2022).

- [27] A. L. Szabó and B. Roy, Metals, fractional metals, and superconductivity in rhombohedral trilayer graphene, *Phys. Rev. B* **105**, L081407 (2022).
- [28] T. Cea, P. A. Pantaleón, V. o. T. Phong, and F. Guinea, Superconductivity from repulsive interactions in rhombohedral trilayer graphene: A kohn-luttinger-like mechanism, *Phys. Rev. B* **105**, 075432 (2022).
- [29] W. Qin, C. Huang, T. Wolf, N. Wei, I. Blinov, and A. H. MacDonald, Functional Renormalization Group Study of Superconductivity in Rhombohedral Trilayer Graphene, arXiv e-prints , arXiv:2203.09083 (2022), arXiv:2203.09083 [cond-mat.supr-con].
- [30] V. Crépel, T. Cea, L. Fu, and F. Guinea, Unconventional superconductivity due to interband polarization, *Phys. Rev. B* **105**, 094506 (2022).
- [31] D.-C. Lu, T. Wang, S. Chatterjee, and Y.-Z. You, Correlated metals and unconventional superconductivity in rhombohedral trilayer graphene: A renormalization group analysis, *Phys. Rev. B* **106**, 155115 (2022).
- [32] A. Jimeno-Pozo, H. Sainz-Cruz, T. Cea, P. A. Pantaleón, and F. Guinea, Superconductivity from electronic interactions and spin-orbit enhancement in bilayer and trilayer graphene, arXiv e-prints , arXiv:2210.02915 (2022), arXiv:2210.02915 [cond-mat.mes-hall].
- [33] F. Wu, A. H. MacDonald, and I. Martin, Theory of phonon-mediated superconductivity in twisted bilayer graphene, *Phys. Rev. Lett.* **121**, 257001 (2018).
- [34] T. J. Peltonen, R. Ojajärvi, and T. T. Heikkilä, Mean-field theory for superconductivity in twisted bilayer graphene, *Phys. Rev. B* **98**, 220504 (2018).
- [35] Y. W. Choi and H. J. Choi, Strong electron-phonon coupling, electron-hole asymmetry, and nonadiabaticity in magic-angle twisted bilayer graphene, *Phys. Rev. B* **98**, 241412 (2018).
- [36] B. Lian, Z. Wang, and B. A. Bernevig, Twisted bilayer graphene: A phonon-driven superconductor, *Phys. Rev. Lett.* **122**, 257002 (2019).
- [37] M. Angeli, E. Tosatti, and M. Fabrizio, Valley jahn-teller effect in twisted bilayer graphene, *Phys. Rev. X* **9**, 041010 (2019).
- [38] F. Wu, E. Hwang, and S. Das Sarma, Phonon-induced giant linear-in- t resistivity in magic angle twisted bilayer graphene: Ordinary strangeness and exotic superconductivity, *Phys. Rev. B* **99**, 165112 (2019).
- [39] F. Schrodi, A. Aperis, and P. M. Oppeneer, Prominent cooper pairing away from the fermi level and its spectroscopic signature in twisted bilayer graphene, *Phys. Rev. Research* **2**, 012066 (2020).
- [40] Y. W. Choi and H. J. Choi, Dichotomy of electron-phonon coupling in graphene moiré flat bands, *Phys. Rev. Lett.* **127**, 167001 (2021).
- [41] Y.-Z. Chou, F. Wu, J. D. Sau, and S. Das Sarma, Acoustic-phonon-mediated superconductivity in rhombohedral trilayer graphene, *Phys. Rev. Lett.* **127**, 187001 (2021).
- [42] Y.-Z. Chou, F. Wu, J. D. Sau, and S. Das Sarma, Acoustic-phonon-mediated superconductivity in bernal bilayer graphene, *Phys. Rev. B* **105**, L100503 (2022).
- [43] S. Firoz Islam, A. Y. Zyuzin, and A. A. Zyuzin, Unconventional superconductivity with preformed pairs in twisted bilayer graphene, arXiv e-prints , arXiv:2208.12039 (2022), arXiv:2208.12039 [cond-mat.supr-con].
- [44] C. Lewandowski, D. Chowdhury, and J. Ruhman, Pairing in magic-angle twisted bilayer graphene: Role of phonon and plasmon umklapp, *Phys. Rev. B* **103**, 235401 (2021).
- [45] C. Lewandowski, S. Nadj-Perge, and D. Chowdhury, Does filling-dependent band renormalization aid pairing in twisted bilayer graphene?, *npj Quantum Materials* **6**, 82 (2021).
- [46] T. Cea and F. Guinea, Coulomb interaction, phonons, and superconductivity in twisted bilayer graphene, *Proceedings of the National Academy of Sciences* **118**, e2107874118 (2021), <https://www.pnas.org/doi/pdf/10.1073/pnas.2107874118>.
- [47] V. o. T. Phong, P. A. Pantaleón, T. Cea, and F. Guinea, Band structure and superconductivity in twisted trilayer graphene, *Phys. Rev. B* **104**, L121116 (2021).
- [48] H. C. Po, L. Zou, A. Vishwanath, and T. Senthil, Origin of mott insulating behavior and superconductivity in twisted bilayer graphene, *Phys. Rev. X* **8**, 031089 (2018).
- [49] V. Kozii, M. P. Zaletel, and N. Bultinck, Superconductivity in a doped valley coherent insulator in magic angle graphene: Goldstone-mediated pairing and Kohn-Luttinger mechanism, arXiv e-prints , arXiv:2005.12961 (2020), arXiv:2005.12961 [cond-mat.str-el].
- [50] S. Chatterjee, T. Wang, E. Berg, and M. P. Zaletel, Intervalley coherent order and isospin fluctuation mediated superconductivity in rhombohedral trilayer graphene, *Nature Communications* **13**, 6013 (2022).
- [51] Z. Dong and L. Levitov, Superconductivity in the vicinity of an isospin-polarized state in a cubic Dirac band, arXiv e-prints , arXiv:2109.01133 (2021), arXiv:2109.01133 [cond-mat.supr-con].
- [52] Z. Dong, A. V. Chubukov, and L. Levitov, Spin-triplet superconductivity at the onset of isospin order in biased bilayer graphene, arXiv e-prints , arXiv:2205.13353 (2022), arXiv:2205.13353 [cond-mat.supr-con].
- [53] See Supplemental Material for: The inter-valley scattering from the Coulomb repulsion and the induced Cooper pairing; The case of the TBG; The case of the RTG and BBG; Screening of the Coulomb interaction.
- [54] V. Crépel and L. Fu, New mechanism and exact theory of superconductivity from strong repulsive interaction, *Science Advances* **7**, eabh2233.
- [55] V. Crépel and L. Fu, Spin-triplet superconductivity from excitonic effect in doped insulators, *Proceedings of the National Academy of Sciences* **119**, e2117735119 (2022), <https://www.pnas.org/doi/pdf/10.1073/pnas.2117735119>.
- [56] F. Guinea and B. Uchoa, Odd-momentum pairing and superconductivity in vertical graphene heterostructures, *Phys. Rev. B* **86**, 134521 (2012).
- [57] R. Roldán, E. Cappelluti, and F. Guinea, Interactions and superconductivity in heavily doped mos_2 , *Phys. Rev. B* **88**, 054515 (2013).
- [58] R. G. Parr, D. P. Craig, and I. G. Ross, Molecular orbital calculations of the lower excited electronic levels of benzene, configuration interaction included, *The Journal of Chemical Physics* **18**, 1561 (1950), <https://doi.org/10.1063/1.1747540>.
- [59] K. Ohno, Some remarks on the pariser-parr-pople method, *Theoretica chimica acta* **2**, 219 (1964).
- [60] N. C. Baird and M. J. S. Dewar, Ground states of σ -bonded molecules. iv. the mindo method and its application to hydrocarbons, *The Journal of Chemical Physics* **50**, 1262 (1969), <https://doi.org/10.1063/1.1671186>.

- [61] J. A. Vergés, E. SanFabián, G. Chiappe, and E. Louis, Fit of pariser-parr-pople and hubbard model hamiltonians to charge and spin states of polycyclic aromatic hydrocarbons, *Phys. Rev. B* **81**, 085120 (2010).
- [62] T. O. Wehling, E. Şaşıoğlu, C. Friedrich, A. I. Lichtenstein, M. I. Katsnelson, and S. Blügel, Strength of effective coulomb interactions in graphene and graphite, *Phys. Rev. Lett.* **106**, 236805 (2011).
- [63] J. M. B. Lopes dos Santos, N. M. R. Peres, and A. H. Castro Neto, Graphene bilayer with a twist: Electronic structure, *Phys. Rev. Lett.* **99**, 256802 (2007).
- [64] R. Bistritzer and A. H. MacDonald, Moiré bands in twisted double-layer graphene, *Proceedings of the National Academy of Sciences* **108**, 12233 (2011), <https://www.pnas.org/doi/pdf/10.1073/pnas.1108174108>.
- [65] J. M. B. Lopes dos Santos, N. M. R. Peres, and A. H. Castro Neto, Continuum model of the twisted graphene bilayer, *Phys. Rev. B* **86**, 155449 (2012).
- [66] M. Koshino, N. F. Q. Yuan, T. Koretsune, M. Ochi, K. Kuroki, and L. Fu, Maximally localized wannier orbitals and the extended hubbard model for twisted bilayer graphene, *Phys. Rev. X* **8**, 031087 (2018).
- [67] A. A. Zibrov, P. Rao, C. Kometter, E. M. Spanton, J. I. A. Li, C. R. Dean, T. Taniguchi, K. Watanabe, M. Serbyn, and A. F. Young, Emergent dirac gullies and gully-symmetry-breaking quantum hall states in *aba* trilayer graphene, *Phys. Rev. Lett.* **121**, 167601 (2018).
- [68] H. Zhou, T. Xie, A. Ghazaryan, T. Holder, J. R. Ehrets, E. M. Spanton, T. Taniguchi, K. Watanabe, E. Berg, M. Serbyn, and A. F. Young, Half- and quarter-metals in rhombohedral trilayer graphene, *Nature* **598**, 429 (2021).
- [69] F. Zhang, B. Sahu, H. Min, and A. H. MacDonald, Band structure of *abc*-stacked graphene trilayers, *Phys. Rev. B* **82**, 035409 (2010).
- [70] T. Nakamura, H. Kim, S. Ichinokura, A. Takayama, A. V. Zotov, A. A. Saranin, Y. Hasegawa, and S. Hasegawa, Unconventional superconductivity in the single-atom-layer alloy Si(111)- $\sqrt{3} \times \sqrt{3}$ -(Tl,Pb), *Phys. Rev. B* **98**, 134505 (2018).
- [71] X. Wu, F. Ming, T. S. Smith, G. Liu, F. Ye, K. Wang, S. Johnston, and H. H. Weiering, Superconductivity in a hole-doped mott-insulating triangular adatom layer on a silicon surface, *Phys. Rev. Lett.* **125**, 117001 (2020).
- [72] F. Ming, X. Wu, C. Chen, K. D. Wang, P. Mai, T. A. Maier, J. Strockoz, J. W. F. Venderbos, C. Gonzalez, J. Ortega, S. Johnston, and H. H. Weiering, Evidence for chiral superconductivity on a silicon surface, arXiv e-prints, arXiv:2210.06273 (2022), [arXiv:2210.06273](https://arxiv.org/abs/2210.06273) [[cond-mat.supr-con](https://arxiv.org/abs/2210.06273)].

Supplementary information for:
**Superconductivity induced by the inter-valley Coulomb scattering in
 few layers of graphene**

**I. THE INTER-VALLEY SCATTERING FROM THE COULOMB REPULSION AND THE INDUCED
 COOPER PAIRING**

We consider the Hamiltonian of the Coulomb repulsion between the p_z electrons within the minimal lattice model for a multilayer of graphene:

$$\hat{H}_{int} = \frac{1}{2} \sum_{\mathbf{R}\mathbf{R}'} \sum_{ij\sigma\sigma'} c_{i\sigma}^\dagger(\mathbf{R}) c_{j\sigma'}^\dagger(\mathbf{R}') V_C^{ij}(\mathbf{R} - \mathbf{R}') c_{j\sigma'}(\mathbf{R}') c_{i\sigma}(\mathbf{R}), \quad (\text{S1})$$

where \mathbf{R} are the coordinates of the Bravais lattice, i, j are the labels of the sub-lattice/layer, $c_{i\sigma}(\mathbf{R})$ is the quantum operator for the annihilation of one electron with spin σ in the p_z orbital localized at the position $\mathbf{R} + \boldsymbol{\delta}_i$, with $\boldsymbol{\delta}_i$ the internal coordinate in the unit cell, and:

$$V_C^{ij}(\mathbf{R} - \mathbf{R}') = \frac{e^2}{4\pi\epsilon |\mathbf{R} - \mathbf{R}' + \boldsymbol{\delta}_i - \boldsymbol{\delta}_j|} \quad (\text{S2})$$

is the Coulomb potential, where e is the electron charge, ϵ is the dielectric constant of the environment, $\epsilon = \epsilon_0$ in the vacuum. Next, we consider the continuum limit of the lattice model, by expanding the operators c as:

$$c_{i\sigma}(\mathbf{R}) \equiv A_c^{1/2} \left[\psi_{i\sigma}^K(\mathbf{R}) e^{i\mathbf{K}\cdot\mathbf{R}} + \psi_{i\sigma}^{K'}(\mathbf{R}) e^{i\mathbf{K}'\cdot\mathbf{R}} \right], \quad (\text{S3})$$

where $A_c = \sqrt{3}a^2/2$ is the area of the unit cell of graphene, $a = 2.46\text{\AA}$ being the lattice constant, K, K' are the non equivalent corners of the BZ and $\psi_{i\sigma}^K(\mathbf{r}), \psi_{i\sigma}^{K'}(\mathbf{r})$ are fermionic operators, which vary smoothly with the continuum position, \mathbf{r} , and represent the valley projections of $c_{i\sigma}(\mathbf{R})$. Replacing the Eq. (S3) into the Eq. (S1), among all the terms one finds the following valley-exchange interaction:

$$\hat{H}_{exc} = A_c^2 \sum_{\mathbf{R}\mathbf{R}'} \sum_{ij\sigma\sigma'} \psi_{i\sigma}^{K,\dagger}(\mathbf{R}) \psi_{j\sigma'}^{K',\dagger}(\mathbf{R}') \psi_{j\sigma'}^K(\mathbf{R}') \psi_{i\sigma}^{K'}(\mathbf{R}) V_C^{ij}(\mathbf{R} - \mathbf{R}') e^{-i\Delta\mathbf{K}\cdot(\mathbf{R}-\mathbf{R}')}, \quad (\text{S4})$$

which describes the inter-valley scattering processes. Note that we used: $V_C^{ij}(\mathbf{R} - \mathbf{R}') = V_C^{ji}(\mathbf{R}' - \mathbf{R})$, in order to remove the factor 1/2 ahead of the Eq. (S4). We exploit the fact that the Fourier envelope of V_C varies slowly for wave vectors close to $\Delta\mathbf{K}$ to assume that the interaction potential of the Eq. (S4) is approximately local:

$$V_C^{ij}(\mathbf{R} - \mathbf{R}') e^{-i\Delta\mathbf{K}\cdot(\mathbf{R}-\mathbf{R}')} \simeq A_c^{-1} v_C^{ij}(\Delta\mathbf{K}) \delta_{\mathbf{R}\mathbf{R}'}, \quad (\text{S5})$$

where:

$$v_C^{ij}(\Delta\mathbf{K}) \equiv A_c \sum_{\mathbf{R}} V_C^{ij}(\mathbf{R} - \mathbf{R}') e^{-i\Delta\mathbf{K}\cdot(\mathbf{R}-\mathbf{R}')}. \quad (\text{S6})$$

Using: $A_c \sum_{\mathbf{R}} \simeq \int d^2\mathbf{r}$ within the previous expression, one obtains:

$$v_C^{ij}(\Delta\mathbf{K}) \simeq \delta^{ij} J \quad , \quad J \equiv \frac{e^2}{2\epsilon|\Delta\mathbf{K}|}, \quad (\text{S7})$$

where the elements in which i, j correspond to the same layer but to different sub-lattices vanish exactly by symmetry (see the App. A), while we neglected the elements in which i, j correspond to different layers, that are suppressed by the factor $e^{-|\Delta\mathbf{K}|d_{ij}}$, $d_{ij} > 0$ being the interlayer distance. Using the Eqs. (S5) and (S7) into the Eq. (S4) and taking the continuum limit finally gives:

$$\begin{aligned} \hat{H}_{exc} &\simeq J \sum_{i\sigma\sigma'} \int d^2\mathbf{r} \psi_{i\sigma}^{K,\dagger}(\mathbf{r}) \psi_{i\sigma'}^{K',\dagger}(\mathbf{r}) \psi_{i\sigma'}^K(\mathbf{r}) \psi_{i\sigma}^{K'}(\mathbf{r}) = \\ &= -J \sum_{i\sigma\sigma'} \int d^2\mathbf{r} \psi_{i\sigma}^{K,\dagger}(\mathbf{r}) \psi_{i\sigma'}^{K',\dagger}(\mathbf{r}) \psi_{i\sigma'}^{K'}(\mathbf{r}) \psi_{i\sigma}^K(\mathbf{r}), \end{aligned} \quad (\text{S8})$$

where we have permuted two operators in the second line, picking up the minus sign. Because $J > 0$, the Eq. (S8) provides an attractive interaction favoring the local occupancy of the two valleys and hence the Cooper pairing with electrons in opposite valleys. In order to figure out the spin structure of the Cooper pairs allowed by the interaction of the Eq. (S8), it is convenient to define the following two-fermions operators:

$$\Psi_{1,-1}^i(\mathbf{r}) = \psi_{i\downarrow}^{K'}(\mathbf{r})\psi_{i\downarrow}^K(\mathbf{r}) \quad , \quad \Psi_{1,0}^i(\mathbf{r}) = \frac{\psi_{i\downarrow}^{K'}(\mathbf{r})\psi_{i\uparrow}^K(\mathbf{r}) + \psi_{i\uparrow}^{K'}(\mathbf{r})\psi_{i\downarrow}^K(\mathbf{r})}{\sqrt{2}} \quad , \quad \Psi_{1,1}^i(\mathbf{r}) = \psi_{i\uparrow}^{K'}(\mathbf{r})\psi_{i\uparrow}^K(\mathbf{r}), \quad (\text{S9a})$$

each of those annihilates a spin triplet Cooper pair, and:

$$\Psi_{0,0}^i(\mathbf{r}) = \frac{\psi_{i\downarrow}^{K'}(\mathbf{r})\psi_{i\uparrow}^K(\mathbf{r}) - \psi_{i\uparrow}^{K'}(\mathbf{r})\psi_{i\downarrow}^K(\mathbf{r})}{\sqrt{2}}, \quad (\text{S9b})$$

which in turns annihilates a spin singlet Cooper pair. Then the Eq. (S8) can be written as:

$$\hat{H}_{exc} \simeq -J \sum_i \int d^2\mathbf{r} \left[\sum_{s=-1,0,1} \Psi_{1,s}^{i,\dagger}(\mathbf{r})\Psi_{1,s}^i(\mathbf{r}) - \Psi_{0,0}^{i,\dagger}(\mathbf{r})\Psi_{0,0}^i(\mathbf{r}) \right], \quad (\text{S10})$$

which is attractive in the triplet channel and repulsive in the singlet one, meaning that only the spin triplet Cooper pairs are stable and, in addition, they are degenerate. The SC OP is purely local:

$$\Delta^i(\mathbf{r}) \propto \langle \Psi_{1,s}^i(\mathbf{r}) \rangle. \quad (\text{S11})$$

Within the BCS theory, the value of T_c can be obtained by looking for nonzero solutions of the linearized gap equation:

$$\Delta^i(\mathbf{r}) = \frac{J}{\beta} \sum_j \int d\mathbf{r}' \sum_{l=-\infty}^{+\infty} \mathcal{G}_{ij}^K(\mathbf{r}, \mathbf{r}'; i\omega_l) \mathcal{G}_{ij}^{K'}(\mathbf{r}, \mathbf{r}'; -i\omega_l) \Delta^j(\mathbf{r}'), \quad (\text{S12})$$

where $\beta = (K_B T)^{-1}$ is the inverse of the temperature, $\omega_l = \pi(2l + 1)/(\hbar\beta)$ are fermionic Matsubara frequencies and $\mathcal{G}^{K,K'}$ are the Green's function for the K, K' valleys, respectively, computed in the normal phase. The Eq. (S12) is written in real space in order to be as general as possible, holding also for the systems that are not translationally invariant, as is the case in the presence of a moiré. In all the cases preserving the translational invariance, then the OP is uniform: $\Delta^i(\mathbf{r}) \equiv \Delta^i$, and the Eq. (S12) reduces to the familiar expression:

$$\Delta^i = \frac{J}{\beta\Omega} \sum_j \sum_{\mathbf{q}} \sum_{l=-\infty}^{+\infty} \mathcal{G}_{ij}^K(\mathbf{q}, i\omega_l) \mathcal{G}_{ij}^{K'}(-\mathbf{q}, -i\omega_l) \Delta^j, \quad (\text{S13})$$

where Ω is the area of the system.

II. THE CASE OF THE TBG

We consider the continuum model of the TBG introduced in the Refs. [63, 64], that describes the hopping between the electrons in opposite layers by means of a local potential having the periodicity of the moiré. This potential breaks the translational invariance within each moiré unit cell and strongly hybridizes the p_z orbitals of the constitutive graphene sheets, generating a number of weakly dispersive minibands at small twist angles. The Bloch's eigenfunction corresponding to the band $E_{n,\mathbf{k}}^K$ of the K -valley can be written as:

$$\Phi_{i,n,\mathbf{k}}^K(\mathbf{r}) = \frac{e^{i\mathbf{k}\cdot\mathbf{r}}}{\sqrt{\Omega}} \sum_{\mathbf{G}} e^{i\mathbf{G}\cdot\mathbf{r}} \phi_{i,n,\mathbf{k}}^K(\mathbf{G}), \quad (\text{S14})$$

where \mathbf{k} is the wave-vector in the moiré BZ, the \mathbf{G} 's are the vectors of the moiré reciprocal lattice and the $\phi_{n,\mathbf{k}}^K(\mathbf{G})$'s are numeric eigenvectors normalized according to: $\sum_{\mathbf{G}} \phi_{i,n,\mathbf{k}}^{K,*}(\mathbf{G})\phi_{i,m,\mathbf{k}}^K(\mathbf{G}) = \delta_{nm}$. The energies and eigenfunctions corresponding to the K' valley are related to the ones at K by the $\mathcal{C}_2\mathcal{T}$ symmetry:

$$E_{n,\mathbf{k}}^{K'} = E_{n,-\mathbf{k}}^K \quad , \quad \Phi_{i,n,\mathbf{k}}^{K'}(\mathbf{r}) = \Phi_{i,n,-\mathbf{k}}^{K,*}(\mathbf{r}). \quad (\text{S15})$$

The Green's functions appearing in the Eq. (S12) are expressed by their spectral decomposition:

$$\mathcal{G}_{ij}^{K/K'}(\mathbf{r}, \mathbf{r}'; i\omega_l) = \sum_{n\mathbf{k}} \frac{\Phi_{i,n,\mathbf{k}}^{K/K'}(\mathbf{r})\Phi_{j,n,\mathbf{k}}^{K/K',*}(\mathbf{r}')}{i\hbar\omega_l - \xi_{n,\mathbf{k}}^{K/K'}}, \quad (\text{S16})$$

where: $\xi_{n,\mathbf{k}}^{K/K'} = E_{n,\mathbf{k}}^{K/K'} - \mu$ and μ is the chemical potential. Using the Eq. (S15), we can write $\mathcal{G}^{K'}$ in terms of the eigenfunctions and energies at K :

$$\mathcal{G}_{ij}^{K'}(\mathbf{r}, \mathbf{r}'; i\omega_l) = \sum_{n\mathbf{k}} \frac{\Phi_{i,n,\mathbf{k}}^{K,*}(\mathbf{r}) \Phi_{j,n,\mathbf{k}}^K(\mathbf{r}')}{i\hbar\omega_l - \xi_{n,\mathbf{k}}^K}. \quad (\text{S17})$$

Because: $\mathcal{G}_{ij}^{K/K'}(\mathbf{r}, \mathbf{r}'; i\omega_l) = \mathcal{G}_{ij}^{K/K'}(\mathbf{r} + \mathbf{R}_m, \mathbf{r}' + \mathbf{R}_m; i\omega_l)$ for any moiré lattice vector \mathbf{R}_m , the solution of the linearized gap equation (S12) is periodic in the moiré unit cell:

$$\Delta^i(\mathbf{r}) = \sum_{\mathbf{G}} \Delta^i(\mathbf{G}) e^{i\mathbf{G}\cdot\mathbf{r}}. \quad (\text{S18})$$

This implies that the Eq. (S12) can be written as:

$$\Delta^i(\mathbf{r}) = J \sum_{kmn} \frac{f(-\xi_{n,\mathbf{k}}^K) - f(\xi_{m,\mathbf{k}}^K)}{\xi_{n,\mathbf{k}}^K + \xi_{m,\mathbf{k}}^K} \Phi_{i,m,\mathbf{k}}^K(\mathbf{r}) \Phi_{i,n,\mathbf{k}}^{K,*}(\mathbf{r}) \int d\mathbf{r}' \sum_j \Phi_{j,m,\mathbf{k}}^{K,*}(\mathbf{r}') \Phi_{j,n,\mathbf{k}}^K(\mathbf{r}') \Delta^j(\mathbf{r}'), \quad (\text{S19})$$

where we have performed the Matsubara sum and introduced the Fermi distribution: $f(x) = (e^{\beta x} + 1)^{-1}$. We can safely assume that the terms with $m \neq n$ barely contribute to the rhs of the Eq. (S19), and write:

$$\Delta^i(\mathbf{r}) \simeq J \sum_{km} \frac{\tanh(\beta\xi_{m,\mathbf{k}}^K/2)}{2\xi_{m,\mathbf{k}}^K} |\Phi_{i,m,\mathbf{k}}^K(\mathbf{r})|^2 \int d\mathbf{r}' \sum_j |\Phi_{j,m,\mathbf{k}}^K(\mathbf{r}')|^2 \Delta^j(\mathbf{r}'). \quad (\text{S20})$$

The Eq. (S20) is equivalent to the following equation for the Fourier amplitudes, $\Delta^i(\mathbf{G})$'s:

$$\Delta^i(\mathbf{G}) = \sum_{j\mathbf{G}'} \Gamma^{ij}(\mathbf{G}, \mathbf{G}') \Delta^j(\mathbf{G}'), \quad (\text{S21})$$

where:

$$\Gamma^{ij}(\mathbf{G}, \mathbf{G}') \equiv \frac{J}{\Omega} \sum_{km} \frac{\tanh(\beta\xi_{m,\mathbf{k}}^K/2)}{2\xi_{m,\mathbf{k}}^K} W_{m,\mathbf{k}}^i(\mathbf{G}) W_{m,\mathbf{k}}^{j,*}(\mathbf{G}'), \quad (\text{S22})$$

and:

$$W_{m,\mathbf{k}}^i(\mathbf{G}) \equiv \sum_{\mathbf{G}''} \phi_{i,n,\mathbf{k}}^{K,*}(\mathbf{G}'') \phi_{i,n,\mathbf{k}}^K(\mathbf{G}'' + \mathbf{G}). \quad (\text{S23})$$

The critical temperature, T_c , is obtained as the value of T such that the largest eigenvalue of the hermitian kernel Γ is equal to 1. The Fourier transform of the corresponding eigenvector, $\Delta^i(\mathbf{G})$, provides the profile of the SC OP in the real space, $\Delta^i(\mathbf{r})$. Because we consider values of the electronic density close to the CNP, we take into account only the contribution of the two central bands to the Eq. (S21).

The Fig. S1 shows the values of T_c as a function of the filling per moiré unit cell, ν , obtained for: $\theta = 1.05^\circ$, which is close to a magic angle, and $\epsilon/\epsilon_0 = 4, 6, 10$, as coded in the inset panel. For the calculation, we have used the parametrization of the TBG given by the Ref. [66] and included the Hartree corrections to both the bands and the eigenfunctions (see [8, 10]). For the realistic values: $\epsilon/\epsilon_0 \sim 4 - 6$, T_c is of the order of 1K and its value increases with the DOS at the Fermi level, N_F , explaining why we find the maximum of T_c at $\nu = 0$, where the bandwidth is minimum (see the Fig. 2 of the manuscript).

The Fig. S2 shows the profile of the SC OP in the moiré unit cell, obtained for: $\theta = 1.05^\circ$, $\epsilon/\epsilon_0 = 4$ and $\nu = -0.5$. Each panel refers to a different sub-lattice/layer combination, where: A, B identify the sub-lattice and 1, 2 the layer. We find that the phase of the OP is always constant, meaning that $\Delta^i(\mathbf{r})$ can be taken as real. It's worth noting that the OP is well localized in the center of the unit cell, the AA -stacked region, which is consistent with the distribution of the charge density in the TBG[64, 65].

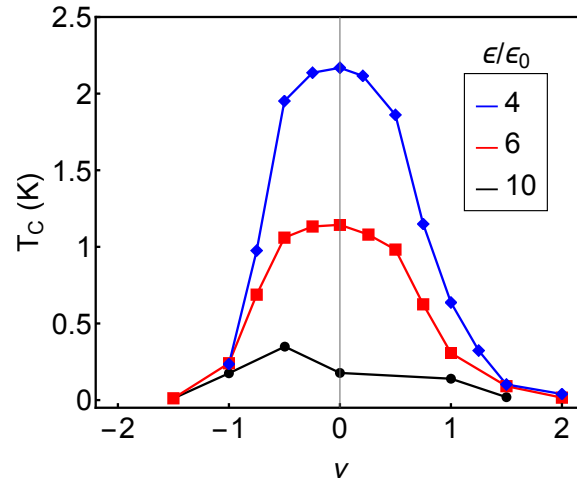


Figure S1. T_c as a function of the filling per moiré unit cell, ν , obtained for: $\theta = 1.05^\circ$ and $\epsilon/\epsilon_0 = 4, 6, 10$.

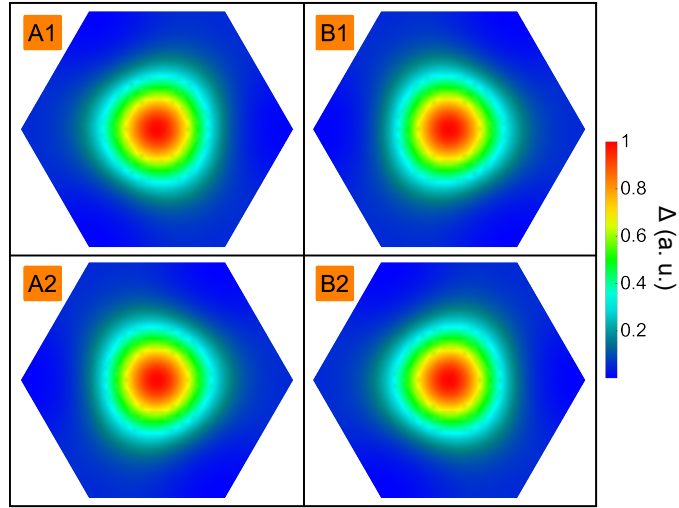


Figure S2. Profile of the SC OP in the moiré unit cell, obtained for: $\theta = 1.05^\circ$, $\epsilon/\epsilon_0 = 4$ and $\nu = -0.5$. Each panel refers to a different sub-lattice/layer combination, where: A, B identify the sub-lattice and 1, 2 the layer.

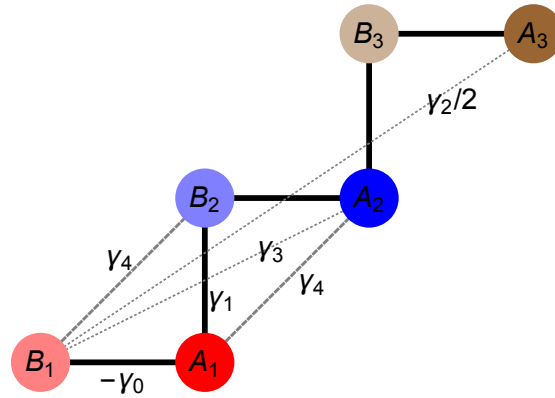


Figure S3. Schematic representation of the stacking arrangement and of the hoppings of the ABC -stacked RTG. The γ_i 's are the hopping amplitudes.

γ_0	γ_1	γ_2	γ_3	γ_4	δ	Δ_2
3.1	0.38	-0.015	0.29	0.141	-0.0105	-0.0023

Table I. Minimal tight-binding parameters of the RTG and BBG.

III. THE CASE OF THE RTG AND BBG

We consider the ABC-stacked RTG and the AB-stacked BBG. The tight binding model of the RTG can be described schematically by the Fig. S3, where the γ_i 's are the hopping amplitudes. A similar scheme can be sketched for the BBG, where the outermost (3rd) layer is missing. We use the low energy continuum model, obtained by expanding the tight-binding Hamiltonian close to the points K, K' . In the momentum space, the Hamiltonian of the RTG is the 6×6 matrix in the basis $(A_1, B_1, A_2, B_2, A_3, B_3)$:

$$H_K(\mathbf{k}) = \begin{pmatrix} \Delta_1 + \Delta_2 & v_0\pi(\mathbf{k}) & -v_4\pi^*(\mathbf{k}) & \gamma_1 & 0 & 0 \\ v_0\pi^*(\mathbf{k}) & \Delta_1 + \Delta_2 + \delta & -v_3\pi(\mathbf{k}) & -v_4\pi^*(\mathbf{k}) & \gamma_2/2 & 0 \\ -v_4\pi(\mathbf{k}) & -v_3\pi^*(\mathbf{k}) & -2\Delta_2 & v_0\pi(\mathbf{k}) & -v_4\pi^*(\mathbf{k}) & \gamma_1 \\ \gamma_1 & -v_4\pi(\mathbf{k}) & v_0\pi^*(\mathbf{k}) & -2\Delta_2 & -v_3\pi(\mathbf{k}) & -v_4\pi^*(\mathbf{k}) \\ 0 & \gamma_2/2 & -v_4\pi(\mathbf{k}) & -v_3\pi^*(\mathbf{k}) & \Delta_2 - \Delta_1 + \delta & v_0\pi(\mathbf{k}) \\ 0 & 0 & \gamma_1 & -v_4\pi(\mathbf{k}) & v_0\pi^*(\mathbf{k}) & \Delta_2 - \Delta_1 \end{pmatrix}, H_{K'}(\mathbf{k}) = H_K^*(-\mathbf{k}), \quad (\text{S24})$$

where $v_i = \gamma_i a \sqrt{3}/(2\hbar)$, $\pi(\mathbf{k}) = \hbar(k_x - ik_y)$, Δ_2 is the potential difference between the middle layer compared to mean potential of the outer layers, δ encodes an on-site potential which is only present at sites B_1 and A_3 since these two atoms do not have a neighbor on the middle layer and Δ_1 is an interlayer bias, which describes the effect of a displacement field perpendicular to the graphene's flakes and opens a gap at the CNP. The Hamiltonian of the BBG is given by the first 4×4 block of the Hamiltonian of the Eq. (S24). We use the values of the γ_i 's, Δ_2 and δ given by the Refs. [28, 67, 68], that we report in the Table I.

Exploiting the translational invariance, we consider the linearized gap equation (S13), with:

$$\mathcal{G}_{ij}^{K/K'}(\mathbf{q}, i\omega_l) = \sum_n \frac{u_{i,n,\mathbf{q}}^{K/K'} u_{i,n,\mathbf{q}}^{K/K',*}}{i\hbar\omega_l - \xi_{n,\mathbf{q}}^{K/K'}}, \quad (\text{S25})$$

where $\mathbf{u}_{n,\mathbf{q}}^{K/K'}$ is the eigenvector of the Hamiltonian of the Eq. (S24) at \mathbf{q} , and: $\mathbf{u}_{n,\mathbf{q}}^{K'} = \mathbf{u}_{n,-\mathbf{q}}^{K,*}$. Replacing the Eq. (S25) into the Eq. (S13) and performing the Matsubara sum, we obtain:

$$\Delta^i = \sum_j \Gamma_{ij} \Delta^j, \quad (\text{S26})$$

where:

$$\Gamma_{ij} \equiv \frac{J}{\Omega} \sum_{qnm} u_{i,n,\mathbf{q}}^K u_{i,m,\mathbf{q}}^{K,*} u_{j,n,\mathbf{q}}^{K,*} u_{j,m,\mathbf{q}}^K \frac{f(-\xi_{m,\mathbf{q}}^K) - f(\xi_{n,\mathbf{q}}^K)}{\xi_{n,\mathbf{q}}^K + \xi_{m,\mathbf{q}}^K}. \quad (\text{S27})$$

Because we consider values of the electronic density such that only one of the two central bands crosses the Fermi surface and the other bands are far away from the Fermi level, we can safely assume that only the states in the partially filled band, \bar{n} , contribute to the kernel, Γ_{ij} , and write:

$$\Gamma_{ij} \simeq \frac{J}{\Omega} \sum_{\mathbf{q}} |u_{i,\bar{n},\mathbf{q}}^K|^2 |u_{j,\bar{n},\mathbf{q}}^K|^2 \frac{\tanh(\beta \xi_{\bar{n},\mathbf{q}}^K)}{2\xi_{\bar{n},\mathbf{q}}^K}. \quad (\text{S28})$$

As we have described in the previous section for the case of the TBG, we look for T_c as the value of T such that the largest eigenvalue of Γ is equal to 1.

Finally, we find that, in the hole-doped regime analyzed in the Fig. 3 of the manuscript, the SC OP is fully localized in the A_3 sub-lattice of the RTG and in the A_2 sub-lattice of the BBG. This is a direct consequence of what shown in the Ref. [69], that the lowest energy states of the gapped RTG (BBG) are fully localized on the A_3 (A_2) or on the B_1 sub-lattice, depending if the system is hole- or electron-doped, respectively.

IV. SCREENING OF THE COULOMB INTERACTION

Here we estimate the screening of the Coulomb interaction by the particle-hole excitations within the Random Phase Approximation (RPA). We consider in particular the case of the RTG, which is translationally invariant, but the arguments can be generalized to the other systems. We consider both the long- and the short-range parts of the interaction.

The bare long-range interaction is described by the potential:

$$v_{LR}(\mathbf{q}) = \frac{e^2}{2\epsilon|\mathbf{q}|}, \text{ for } \mathbf{q} \simeq 0. \quad (\text{S29})$$

Note that v_{LR} does not depend on the internal indices of sub-lattice/layer, since the long-range interaction is an effective charge-charge repulsion. The screening is given by the usual Thomas-Fermi formula:

$$\tilde{v}_{LR}(\mathbf{q}) = \frac{1}{v_{LR}^{-1}(\mathbf{q}) - \Pi(\mathbf{q})} \simeq -\frac{1}{\Pi(0)}, \quad (\text{S30})$$

where $\Pi(\mathbf{q})$ is the charge susceptibility that, at $\mathbf{q} = 0$, can be written as:

$$\Pi(0) = \frac{4}{\Omega} \sum_{\mathbf{k}nm} |\mathbf{u}_{m,\mathbf{k}}^K \cdot \mathbf{u}_{n,\mathbf{k}}^K|^2 \frac{f(\xi_{n,\mathbf{k}}^K) - f(\xi_{m,\mathbf{k}}^K)}{\xi_{n,\mathbf{k}}^K - \xi_{m,\mathbf{k}}^K}, \quad (\text{S31})$$

where the factor of 4 comes from the spin/valley degeneracy. The leading contribution to $\Pi(0)$ is the intra-band contribution corresponding to the band crossing the Fermi level, \bar{n} , so we can write:

$$\Pi(0) \simeq \frac{4}{\Omega} \sum_{\mathbf{k}} f'(\xi_{\bar{n},\mathbf{k}}^K) \xrightarrow{T \rightarrow 0} -N_F. \quad (\text{S32})$$

If the Fermi level matches the VHS, then $N_F \rightarrow \infty$ and hence $\tilde{v}_{LR}(\mathbf{q}) \rightarrow 0$.

To derive the screening of the short-range interaction, namely of J , it is convenient to consider the Hamiltonian of the Eq. (S8) and write the corresponding euclidean action:

$$S_{exc} = J \sum_{i\sigma\sigma'} \int dx \psi_{i\sigma}^{K,\dagger}(x) \psi_{i\sigma}^{K'}(x) \psi_{i\sigma'}^{K',\dagger}(x) \psi_{i\sigma'}^K(x), \quad (\text{S33})$$

where $x = (\mathbf{r}, \tau)$ and τ is the imaginary time. When computing the partition function, S_{exc} can be decoupled by introducing a set of complex Hubbard-Stratonovich (HS) fields, Φ_i , according to:

$$\begin{aligned} e^{-\frac{1}{\hbar} S_{exc}} &= \int \prod_i \mathcal{D}[\Phi_i, \Phi_i^*] \exp \left\{ -\frac{\hbar}{J} \sum_i \int dx |\Phi_i(x)|^2 + i \sum_{i\sigma} \int dx [\bar{\psi}_{i\sigma}^K(x) \psi_{i\sigma}^{K'}(x) \Phi_i(x) + c.c.] \right\} = \\ &= \int \prod_i \mathcal{D}[\Phi_i, \Phi_i^*] \exp \left\{ \frac{\hbar}{J} \sum_{iq} |\Phi_i(q)|^2 + i \sqrt{\frac{K_B T}{\hbar \Omega}} \sum_{i\sigma k k'} [\bar{\psi}_{i\sigma}^K(k) \psi_{i\sigma}^{K'}(k') \Phi_i(k - k') + c.c.] \right\}, \end{aligned} \quad (\text{S34})$$

where $\psi, \bar{\psi}$ are grassmanian numbers, $q = (\mathbf{q}, i\Omega_l)$, $\Omega_l = 2\pi l K_B T / \hbar$ are bosonic Matsubara frequencies, and $k = (\mathbf{k}, i\omega_l)$. The Eq. (S34) defines the following self-energy:

$$\Sigma_{\sigma\sigma'}^{ij}(k - k') \equiv -i \delta_{ij} \delta_{\sigma\sigma'} \sqrt{\frac{K_B T}{\hbar \Omega}} \begin{pmatrix} 0 & \Phi_i(k - k') \\ \Phi_i^*(k' - k) & 0 \end{pmatrix}, \quad (\text{S35})$$

where the 2×2 matrix acts in the valley space. Integrating out the Fermionic fields, we obtain the effective action for the HS fields that, at the gaussian level, is given by:

$$\begin{aligned} \frac{1}{\hbar} S_{eff}[\Phi, \Phi^*] &= \frac{\hbar}{J} \sum_{iq} |\Phi_i(q)|^2 + \frac{\hbar^2}{2} \sum_{kq} \text{Tr} \{ \mathcal{G}(k + q) \Sigma(q) \mathcal{G}(k) \Sigma(-q) \} = \\ &= \hbar \sum_{ijq} \tilde{J}_{ij}^{-1}(q) \Phi_i^*(q) \Phi_j(q), \end{aligned} \quad (\text{S36})$$

where:

$$\tilde{J}_{ij}^{-1}(q) \equiv \frac{\delta_{ij}}{J} - 2 \frac{K_B T}{\Omega} \sum_k \mathcal{G}_{ij}^K(k+q) \mathcal{G}_{ji}^{K'}(k) \quad (\text{S37})$$

is the inverse of the screened J . Note that \tilde{J} is a matrix in the sub-lattice/layer indices. This is not surprising, since J is a matrix too, but proportional to the identity. We focus on the $q = 0$ limit. Using the spectral decomposition of the Green's functions $\mathcal{G}^K, \mathcal{G}^{K'}$ and performing the Matsubara sums, we finally obtain:

$$\tilde{J}_{ij}^{-1} \equiv \tilde{J}_{ij}^{-1}(0) = \frac{\delta_{ij}}{J} - \frac{2}{\Omega} \sum_{\mathbf{k}nm} [u_{ni}^K(\mathbf{k}) u_{mi}^K(-\mathbf{k})] [u_{nj}^K(\mathbf{k}) u_{mj}^K(-\mathbf{k})]^* \times \frac{f(\xi_{m,-\mathbf{k}}^K) - f(\xi_{n,\mathbf{k}}^K)}{\xi_{m,-\mathbf{k}}^K - \xi_{n,\mathbf{k}}^K}. \quad (\text{S38})$$

Note that, since generally $\xi_{n,-\mathbf{k}}^K \neq \xi_{n,\mathbf{k}}^K$, the intra-band contribution to the rhs of the Eq. (S38) is not expected to provide a relevant weight and, consequently, the strength of the short-range interaction is not expected to be strongly screened as compared to its bare value, J . This is a consequence of the fact that, at the level of the RPA, the processes contributing to screen J are particle-hole excitations with the particle and the hole propagating in opposite valleys.

In order to give a quantitative estimate of the screening effects, we consider the RTG with $\Delta_1 = 50\text{meV}$ and $n_e = -0.75 \times 10^{12}\text{cm}^{-2}$. For this choice of the parameters, the Fermi level matches the VHS. Using a very small temperature, $T = 10^{-6}\text{K}$, we obtain:

$$\tilde{v}_{LR}(0) = 0.01\text{eV}\text{\AA}^2 \quad , \quad \tilde{J} = \begin{pmatrix} 13.22 & 0 & 0 & 0.02 & 0 & 0 \\ 0 & 13.16 & 0 & 0 & -0.01 & 0 \\ 0 & 0 & 13.07 & 0 & 0 & 0.01 \\ 0.02 & 0 & 0 & 13.22 & 0 & 0 \\ 0 & -0.01 & 0 & 0 & 9.43 & 0 \\ 0 & 0 & 0.01 & 0 & 0 & 13.22 \end{pmatrix} \text{eV}\text{\AA}^2. \quad (\text{S39})$$

This means that: i) the long-range interaction is almost completely screened, resulting order of magnitudes smaller than J . Then one can assume that the long-range effects are not relevant. ii) \tilde{J} is approximately diagonal and its diagonal elements barely deviates from the bare value: $J = 13.25\text{eV}\text{\AA}^2$, which allows one to safely neglect the screening of the short-range interaction, assuming: $\tilde{J}_{ij} \simeq J\delta_{ij}$.

Appendix A

We show that, if i, j correspond to the same layer but to different sub-lattices, then:

$$\sum_{\mathbf{R}} V_C^{ij}(\mathbf{R}) e^{-i\Delta K \cdot \mathbf{R}} \propto \sum_{\mathbf{R}} \frac{e^{-i\Delta K \cdot \mathbf{R}}}{|\mathbf{R} + \boldsymbol{\delta}_i - \boldsymbol{\delta}_j|} = 0, \quad (\text{S1})$$

where: $\mathbf{R} = n_1 \mathbf{R}_1 + n_2 \mathbf{R}_2$, with n_1, n_2 integer, and $\mathbf{R}_1 = a(1, \sqrt{3})/2$, $\mathbf{R}_2 = a(-1, \sqrt{3})/2$ are the two unit vectors of the Bravais lattice of the monolayer graphene, as shown in the Fig. S4(a). Without loss of generality, we can assume that the atomic displacement between the two sub-lattices in each unit cell is: $\boldsymbol{\delta} \equiv \boldsymbol{\delta}_i - \boldsymbol{\delta}_j = a(0, 1)/\sqrt{3}$, and that: $\Delta K = 2\pi(1, -\sqrt{3})/(3a)$ (see the Fig. S4(b)).

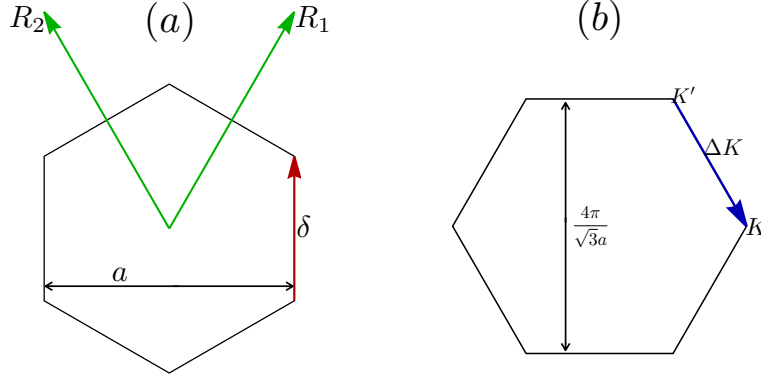


Figure S4. (a) Unit cell of the monolayer graphene. \mathbf{R}_1 and \mathbf{R}_2 are the unit vectors of the Bravais lattice and $\boldsymbol{\delta}$ is the atomic displacement between the two sub-lattices. (b) Brillouin zone of the monolayer graphene. K, K' are the two non equivalent corners and $\Delta K = K - K'$.

Considering that, for any n integer, the Bravais lattice is invariant under the rotation by $2n\pi/3$, C_n , we can write the sum in the Eq. (S1) as:

$$\sum_{\mathbf{R}} \frac{e^{-i\Delta K \cdot \mathbf{R}}}{|\mathbf{R} + \boldsymbol{\delta}|} = \frac{1}{3} \sum_{\mathbf{R}} \left[\frac{e^{-i\Delta K \cdot \mathbf{R}}}{|\mathbf{R} + \boldsymbol{\delta}|} + \frac{e^{-i\Delta K \cdot (C_1 \mathbf{R} - \mathbf{R}_1)}}{|C_1 \mathbf{R} - \mathbf{R}_1 + \boldsymbol{\delta}|} + \frac{e^{-i\Delta K \cdot (C_2 \mathbf{R} - \mathbf{R}_2)}}{|C_2 \mathbf{R} - \mathbf{R}_2 + \boldsymbol{\delta}|} \right], \quad (\text{S2})$$

where, in addition to the rotation $C_1(C_2)$, we have performed a translation by $-\mathbf{R}_1(-\mathbf{R}_2)$. Noting that:

$$\boldsymbol{\delta} - \mathbf{R}_{1,2} = C_{1,2} \boldsymbol{\delta} \quad , \text{ and: } \quad e^{-i\Delta K \cdot C_{1,2} \mathbf{R}} = e^{-i\Delta K \cdot \mathbf{R}}, \quad (\text{S3})$$

then we can write the Eq. (S2) as:

$$\sum_{\mathbf{R}} \frac{e^{-i\Delta K \cdot \mathbf{R}}}{|\mathbf{R} + \boldsymbol{\delta}|} = \sum_{\mathbf{R}} \frac{e^{-i\Delta K \cdot \mathbf{R}}}{|\mathbf{R} + \boldsymbol{\delta}|} \times \left(\frac{1 + e^{i\Delta K \cdot \mathbf{R}_1} + e^{i\Delta K \cdot \mathbf{R}_2}}{3} \right) = 0, \quad (\text{S4})$$

as it follows by: $1 + e^{i\Delta K \cdot \mathbf{R}_1} + e^{i\Delta K \cdot \mathbf{R}_2} = 1 + e^{-2i\pi/3} + e^{2i\pi/3} = 0$.